Applied Catalysis B: Environment and Energy 352 (2024) 124059

Contents lists available at ScienceDirect

Applied Catalysis B: Environment and Energy

journal homepage: www.elsevier.com/locate/apcatb

Hydrodeoxygenation of lignin-derived phenols into cycloalkanes by atomically dispersed Pt-polyoxometalate catalysts

Xueying Gao [a,b], Rumin Ma [a], Zhenzhen Liu [a,c], Shuizhong Wang [a], Yulong Wu [b,d,*], Guoyong Song [a,**]

[a] State Key Laboratory of Efficient Production of Forest Resources, Beijing Key Laboratory of Lignocellulosic Chemistry, Beijing Forestry University, Beijing 100083, China
[b] Institute of Nuclear and New Energy Technology, Tsinghua University, Beijing 100084, China
[c] International Centre for Bamboo and Rattan, Beijing 100102, China
[d] School of Chemical Engineering and Technology, Xinjiang University, Xinjiang 830046, China

ARTICLE INFO

Keywords:
Lignin
Hydrodeoxygenation
Cycloalkanes
Polyoxometalate
Atomically dispersed Pt

ABSTRACT

We report atomically dispersed Pt sites anchored on polyoxometalate cesium salts as robust and durable catalysts for upgrading lignin into hydrocarbons at relatively mild conditions. Experimental results and DFT calculations cross-validate the catalytic performance, considering the porosity, acidity, H_2 storage capacity, and HOMO-LUMO energy gap of these catalysts. The optimal $Pt_{0.4}$/CsPW-H_2 catalyst enables the hydrodeoxygenation (HDO) of a diverse range of lignin-derived phenolics into hydrocarbons with up to 97% yield at the conditions of 150 °C and 0.1–2 MPa H_2. A lignin oil from the reductive catalytic fractionation (RCF) of Eucalyptus wood can be transformed into cyclohexanes with a 32.7 wt% yield under a solvent-free condition. This catalyst demonstrates excellent reusability in the HDO of 4-propyl guaiacol for 20 cycles, achieving a 15095 $mol_{propylcyclohexane}$ mol_{Pt}^{-1} total turnover number (TON). This work broadens the horizons of designing highly efficient catalytic systems aimed at sustainably producing liquid fuels from lignin.

1. Introduction

In a climate warming setting, with more soaring global demand for reducing CO_2 emissions and promoting carbon neutralization, biomass has garnered considerable attention worldwide owing to its unique carbon-negative emissions while combining carbon capture and storage technologies to produce liquid fuels [1–3]. Lignin, the main component of lignocellulose biomass (15–30 wt%), is one of the few renewable aromatic resources in nature. Unfortunately, it is often disregarded, either left to decay in the field or directly incinerated to generate energy [4–6]. Lignin's building blocks consist of phenylpropanoid units, which boast high aromaticity, low oxygen content, and natural C9 skeletons, making lignin a promising alternative and complement to fossil resources compared to cellulose and hemicellulose [6,7]. However, the complex and irregular structure of lignin presents challenges for its conversion [8]. Despite these obstacles, significant progress has been made in developing lignin valorization technologies aimed at addressing these complexities. [9–11].

Reductive catalytic fractionation (RCF) of biomass, known as the "lignin first" strategy, has recently emerged as a new biorefinery paradigm for lignin valorization [10,12]. Such a procedure can efficiently depolymerize native lignin in biomass matrix into phenolic monomers, dimers, and oligomers, together leaving carbohydrate pulp with high retentions [12,13]. The resulting lignin-derived components are theoretically optimal feedstocks for producing jet-fuel range cycloalkanes via hydrodeoxygenation (HDO), owing to their complete aromaticity, higher energy density, and good fluidity [14–19]. Grilc and coworkers investigated the activity and mechanisms of the HDO of lignin model compound eugenol over commercially available metal catalysts at 275 °C and 5 MPa H_2 [20]. Schîth et al. developed a PtCo/NOMC-2 catalyst for the HDO of "real-world" biomass-derived phenolic streams, by which complete deoxygenation was achieved under conditions of 300 °C and 10 MPa H_2 [19]. Ma et al. demonstrated that the Ni/SZ catalyst can effectively convert lignin-derived phenolics into alkanes and aromatics at 300 °C and 5 MPa H_2 [21]. Wang et al. reported Au/Nb_2O_5-catalyzed HDO of lignin-depolymerized oils, from which high selectivity towards

* Corresponding author at: Institute of Nuclear and New Energy Technology, Tsinghua University, Beijing 100084, China
** Corresponding author.
E-mail addresses: wylong@tsinghua.edu.cn (Y. Wu), songg@bjfu.edu.cn (G. Song).

https://doi.org/10.1016/j.apcatb.2024.124059
Received 9 December 2023; Received in revised form 4 April 2024; Accepted 7 April 2024
Available online 9 April 2024

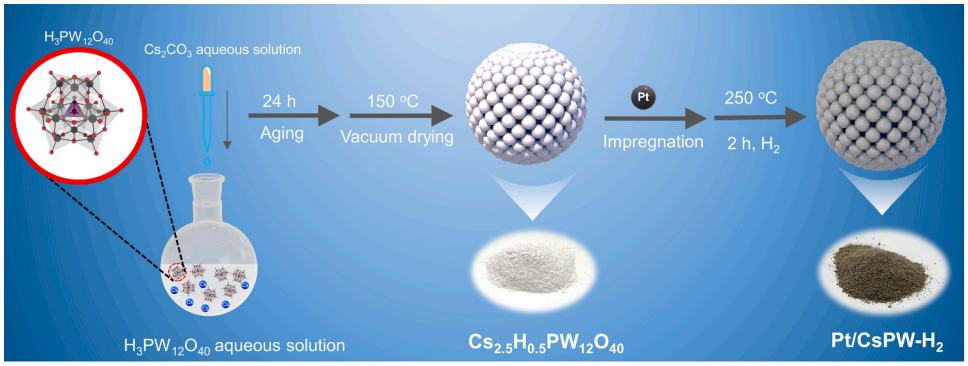

Scheme 1. Schematic illustration of the preparation of $Pt_{0.4}$/CsPW-H_2.

phenolics was realized at 300 °C and 6.5 MPa H_2 [18]. Li and co-worker developed a series of MoS_{2-x} incorporated Co [14,16] and Pt catalysts [22], by which poplar lignin oils were hydrodeoxygenated to aromatics or naphthenic hydrocarbons at 260 °C and 3–4 MPa H_2. Rinaldi et al. employed a phosphidated Ni/SiO_2 catalyst to upgrade lignin oils, where the selectivity towards aliphatic or aromatic products could be regulated by H_2 pressure (0.5–5 MPa) and temperature (300–350 °C) [15]. Recently, we developed a sub-nanometric Ru catalyst, which exhibited exceptional performance in the HDO of miscanthus lignin-derived bio-phenolics to cyclohexanes under 200 °C and 3 MPa H_2 [23]. Of note, the aforementioned cases necessitated rigorous reaction conditions, such as elevated temperatures (200–350 °C) and high H_2 pressure (3–10 MPa), which resulted in energy-extensive consumption and the demand for equipment [24,25].

The effectiveness of Keggin-structured polyoxometalates has been illustrated in numerous biomass conversions [26] and the HDO of various oxygenates [27–31], due to their strong and resilient acidic sites, exceptional redox properties, and remarkable stability [32,33]. Kozhevnikov and co-workers reported that a phosphotungstic cesium salt-supported Pt catalyst can efficiently catalyze the HDO of ethers [27] and ketones [31] under mild reaction conditions (<100 °C, <1 bar H_2). Sautet and Yan demonstrated that Pt single-atom catalysts stabilized by polyoxometalates can weaken the H_2 adsorption energy compared to Pt clusters due to the metal-support effects, which suppress the Pt single-atoms aggregation and does not affect the reactivity, thus resulting in small apparent activation barriers in several hydrogenation reactions [29]. Very recently, Deng and co-workers found that the combination of Pt/C and polyoxometallate acid enabled the upgrading of lignin bio-oil to hydrocarbons in water under mild conditions, where polyoxometallate acid served as the H_2 buffer and carrier. However, the good water solubility of polyoxometallate acid may hinder its recovery process [34]. Given that lignin tends to diminish H_2 absorption capacity in the Al_2O_3-supported Pt catalyst [35], catalyst supports with H_2 buffering capacity, such as polyoxometalate, would be the ideal selection for the development of lignin HDO catalysts.

Motivated by the above-mentioned results, we herein presented a family of low-loaded, atomically dispersed Pt catalysts supported on Keggin polyoxometalate cesium salts, which featured well-defined porous structure, strong acidity, high H_2 storage capacity, and relatively small HOMO-LUMO energy gap, as evidenced by experimental characterizations and DFT calculations. The phosphotungstic cesium-supported Pt catalyst, $Pt_{0.4}$/CsPW-H_2, exhibited remarkable activity in the HDO of a series of lignin-derived monomeric and dimeric phenols, thus giving corresponding hydrocarbons in high yield under relatively mild conditions (0.1–2 MPa H_2, 150 °C) with substrate/Pt molar ratios up to 909. This catalyst demonstrated good reusability in continuous injection reactions for at least 80 hours, achieving a high total turnover number (TON) of 15095 $mol_{propylcyclohexane}$ mol_{Pt}^{-1}. By feeding wood-derived RCF lignin oils, effective HDO successfully occurred and impressive yields of cycloalkane derivatives were acquired over this catalyst.

2. Experimental section

2.1. Catalyst preparation

The reactions between Cs_2CO_3 with polyoxometalates, including phosphotungstic acid ($H_3PW_{12}O_{40}$, HPW), phosphomolybdic acid ($H_3PMo_{12}O_{40}$, HPM), and tungstosilicic acid ($H_4SiW_{12}O_{40}$, HSiW), resulting in corresponding polyoxometalate cesium salts $Cs_xH_{3-x}PW_{12}O_{40}$ (CsPW), $Cs_xH_{3-x}PMo_{12}O_{40}$ (CsPMo) and $Cs_xH_{4-x}SiW_{12}O_{40}$ (CsSiW), respectively. In a standard procedure, an aqueous solution of Cs_2CO_3 (1.53 g in 10 mL water) was added to an aqueous solution of $H_3PW_{12}O_{40}$ (10.8 g in 10 mL water) at 40 °C dropwise. The as-obtained white precipitate was aged for 24 hours at room temperature before undergoing slow evaporation in a rotary evaporator at 45 °C. The as-obtained CsPW was dried under vacuum before use.

Pt_x/CsPW-H_2 catalysts were obtained by the incipient wetness method. The as-prepared CsPW was dipped into a benzene solution containing platinum bis(acetylacetonate) ($Pt(acac)_2$). Then, the mixture was stirred at room temperature for 1 h, which upon the evaporation of solvent, and drying at 150 °C under vacuum, to afford Pt_x/CsPW. A flow H_2-treatment of Pt_x/CsPW at 250 °C for 2 h generated Pt_x/CsPW-H_2 catalysts, which were stored under N_2 at ambient temperature before use. The Ru_x/CsPW-H_2 were prepared using a similar approach by employing $RuCl_3 \cdot 3\ H_2O$ as the metal precursor.

2.2. Catalyst characterization

The inductively coupled plasma-optical emission spectroscopy (ICP-OES) studies were performed on Agilent 7700 ICP-MS. The X-ray powder diffraction (XRD) patterns were obtained on a Rigaku UltimaIV diffractometer. X-ray photoelectron spectroscopies (XPS) were conducted on a Thermo ESCALAB 250XI machine. High resolution transmission electron microscopy (HRTEM) images were obtained over a JEOL JEM-F200. N_2 adsorption-desorption isotherms were collected on a Builder SSA-7000 specific surface and aperture analyzer. Fourier Transform Infrared Spectrometer (FTIR) spectra were gained on a PerkinElmer Frontier spectrometer. Thermogravimetric analyses (TGA) were conducted over the TGA 5500. The infrared spectra of adsorbed pyridine (Py-IR) were obtained on a Thermo Scientific Nicolet iS50 Frontier spectrometer. Temperature-programmed desorption of hydrogen (H_2-TPD) and ammonia (NH_3-TPD) was performed on Micromeritics AutoChem II 2920 chemical adsorption instruments. The high-angle annular-dark-field scanning transmission electron microscopy (HAADF-STEM) images were recorded at Titan ThemisZ STEM. The X-ray absorption characteristics were examined at the L-edge of Pt using X-ray absorption spectra (XAS), which encompassed both X-ray absorption near-edge structure (XANES) and extended X-ray absorption fine structure (EXAFS) spectra. These measurements were conducted at

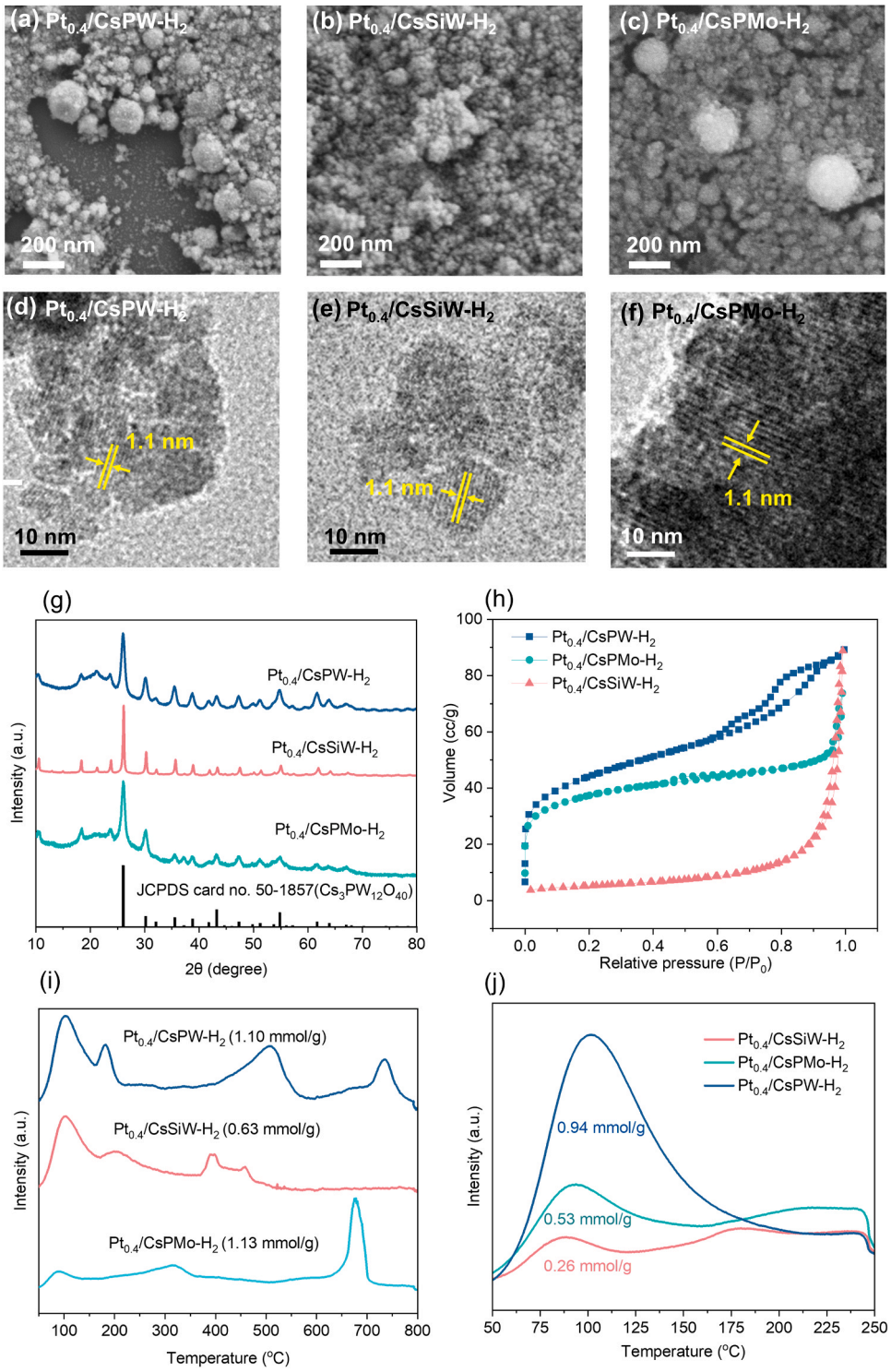

Fig. 1. Characterizations of various polyoxometalate supported catalysts. (a-c) STEM images. (d-f) HRTEM images. (g) XRD patterns. (h) N_2 physisorption isotherms curves based on BJH method. (i) NH_3-TPD spectra. (j) H_2-TPD profiles.

the 1W1B station located within the Beijing Synchrotron Radiation Facility (BSRF) in China. The 2D HSQC NMR spectra were acquired on a Bruker AVIII 400 MHz spectrometer.

2.3. Calculation details

Calculations in this work were accomplished by using the DMol^3 program [36,37], which based on density functional theory (DFT) within the Perdew-Burke-Emzerh of generalized gradient approximation (GGA-PBE) scheme approach. GGA-PBE is a refinement of the approximation methods used in DFT to more accurately describe the exchange-correlation energy of a system based on its electron density and the gradients of that density [38]. DFT semicore pseudopotentials were used together with double numerical plus polarization (DNP) functions, which were used to detailly describe the electron behavior. Energy and force were programmed with 10^{-5} Ha and 0.001 Ha/Å respectively. Displacement convergence criteria has been set at 0.005 Å. An effective core potential (ECP) was used for core treatment and

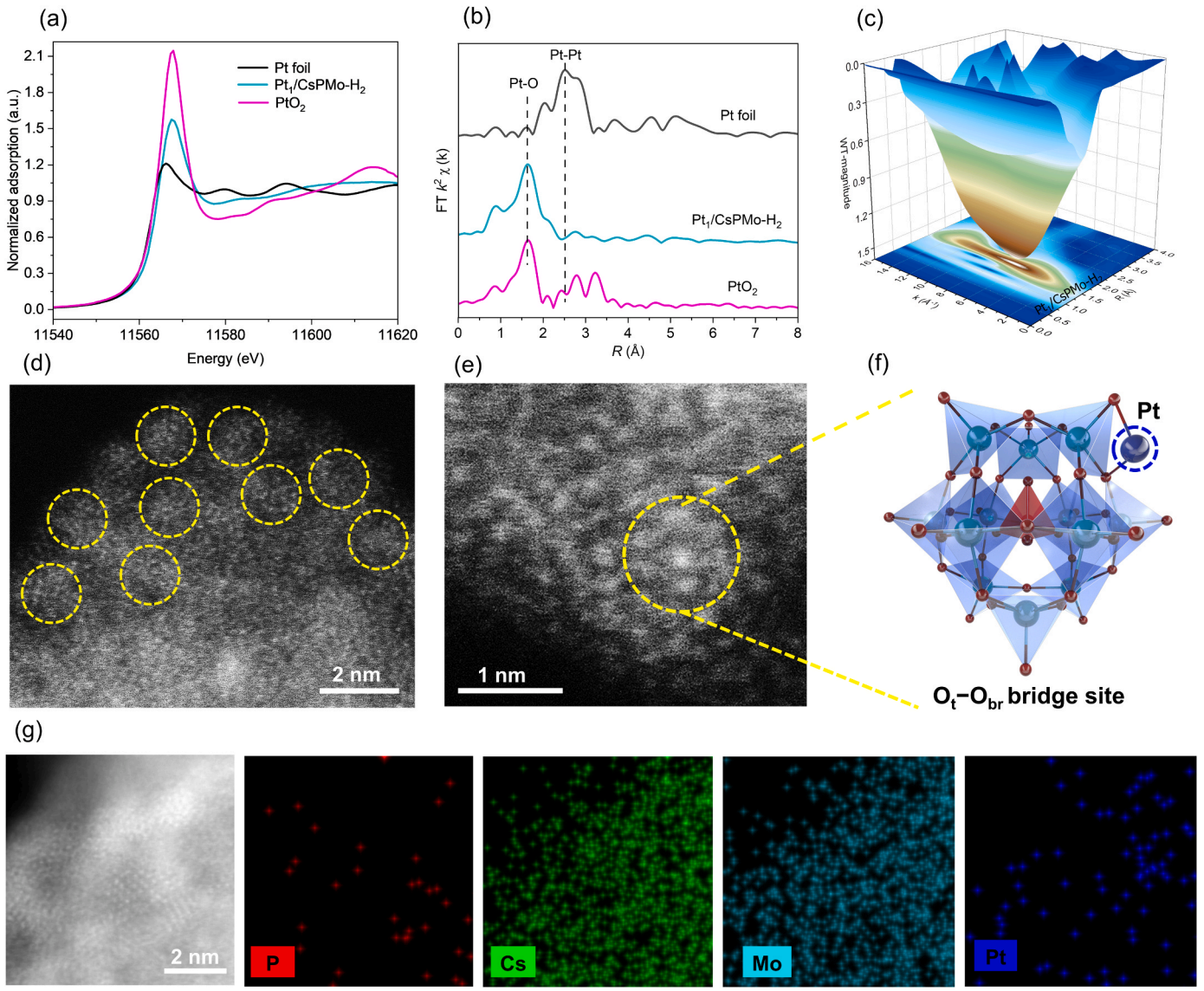

Fig. 2. Characterizations of $Pt_1/CsPMo\text{-}H_2$. (a) The Pt L_3-edge XANES spectra. (b) FT of the k^2-weighted EXAFS spectra. (c) WT for the k^2-weighted EXAFS signals. (d)&(e) Magnified atomic-resolution HAADF-STEM image. (f) The illustration of the structure model of isolated Pt atom in $O_t{-}O_{br}$ bridge site of $[PMo_{12}O_{40}]^{3+}$. (g) Corresponding EDS elemental mapping for the distribution of P, Cs, Mo and Pt elements.

4.4 mm as the space cutoff radius.

2.4. Catalyst evaluation

The HDO of 4-propylguaiacol was performed in a 50 mL Parr autoclave reactor. In a quintessential procedure, a mixture containing 4-propylguaiacol (166 mg, 1 mmol), catalyst (50 mg), bicyclohexyl (an internal standard), and dodecane (3 mL) was introduced into the reactor, which was then purged with nitrogen three times and pressurized with hydrogen at a pressure of 2 MPa. Afterward, the reactor was heated to the target temperature for a specific duration with magnetic stirring. To prevent the loss of alkane products with low boiling points, the reactor was cooled to −18 °C and retained overnight before collection and measurement. The liquid products were carefully collected, and the solid residues were filtered out using Nylon syringe filters with a pore size of 0.22 μm before analysis. The identification and quantification of the liquid products were determined by GC-MS (Shimaduzu GCMS-QP2010SE) and GC (Shimaduzu GC-2010) equipped with HP-5 MS column and HP-5 column, respectively.

2.5. Catalytic conversion of Eucalyptus-derived lignin oil

A combination of Eucalyptus sawdust (10 g), Ru/C (100 mg, Ru loading is 5 wt%) and methanol (120 mL) was charged into a 300 mL autoclave, which was subsequently sealed, purged with N_2 three times, and pressurized with 3.0 MPa of H_2. The RCF experiment was conducted at a temperature of 230 °C for 6 hours with vigorous stirring. After the reaction, the liquid phase was collected by filtration, which upon the removal of methanol gave a crude lignin oil. Biomass composition analysis indicated that *ca.* 96 wt% of cellulose and 61 wt% of hemicellulose were retained in the solid phase. Extracting lignin oily products by CH_2Cl_2/water resulted in lignin-derived monomers, dimers, and oligomers in the organic phase and a small number of sugars in the aqueous phase. Subsequent removal of CH_2Cl_2 afforded 2.09 g of lignin-depolymerized products, corresponding to 91.0 wt% of lignin in Eucalyptus sawdust. Based on GC analyses, 807 mg (*ca.* 0.68 mmol) of monomeric products were identified in the lignin oily products. Phenolic dimers in lignin oil are identified by GC-MS after derivatization by the reaction with *N,O*-bis(trimethylsilyl)trifluoroacetamide (BSTFA) in tetrahydrofuran at 65 °C for one hour under nitrogen.

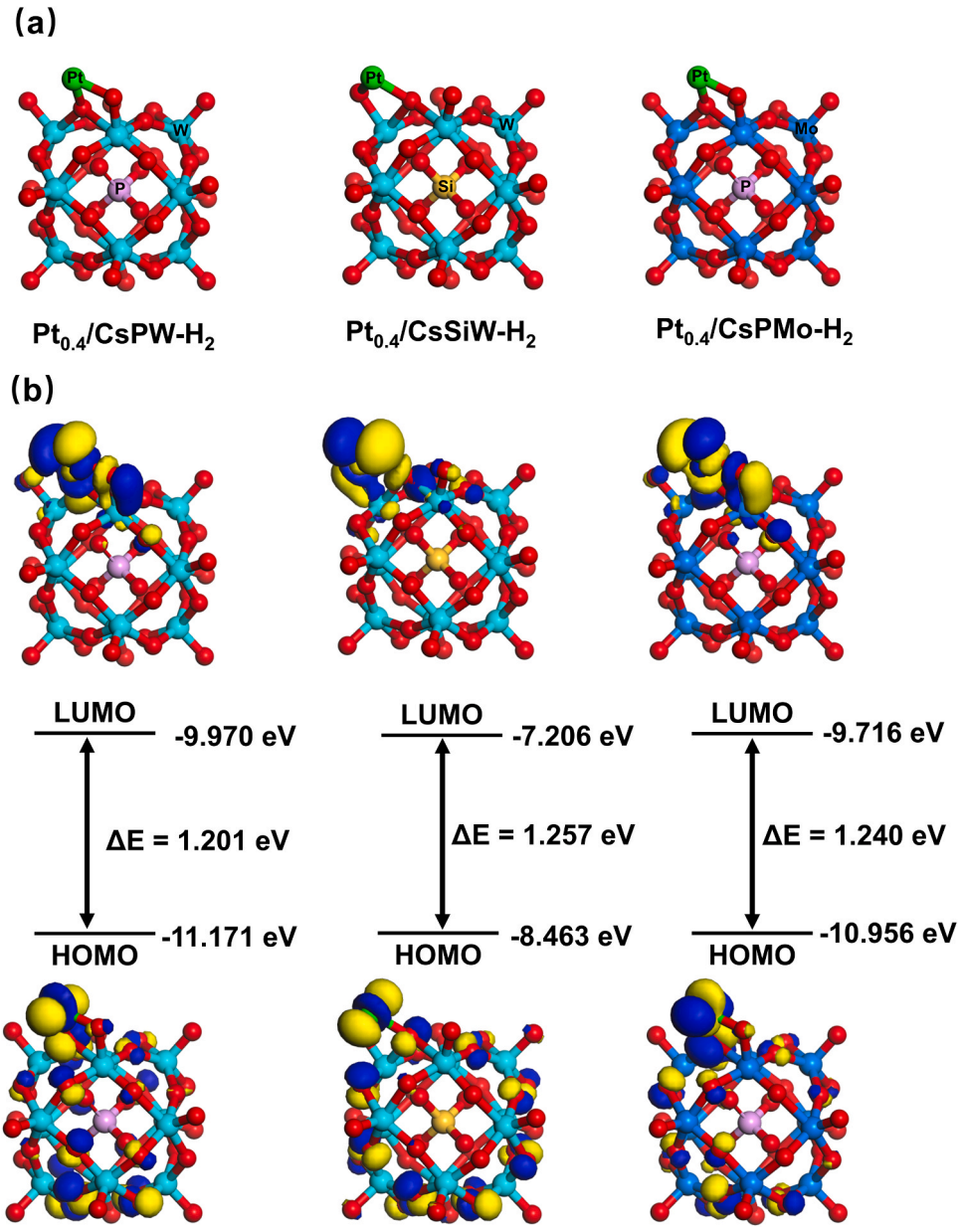

Fig. 3. (a) Structures models and (b) the calculated HOMO and LUMO orbitals and energy levels of $Pt_{0.4}/CsPW\text{-}H_2$, $Pt_{0.4}/CsSiW\text{-}H_2$, and $Pt_{0.4}/CsPMo\text{-}H_2$.

Catalytic conversion of Eucalyptus-derived lignin oils was performed under *solvent-free* conditions using lignin oils (1.7 g) and $Pt_{0.4}/CsPW\text{-}H_2$ (800 mg) in batch reactor under 150 °C, 2 MPa H_2 for 24 h. After the reaction, the resultant products were dissolved in $CDCl_3$, which was then analyzed by GC, GC/MS, and 2D HSQC NMR spectroscopy.

3. Results and discussion

3.1. Synthesis and characterization of catalysts

Polyoxometalates with Keggin structure, such as phosphotungstic acid ($H_3PW_{12}O_4$, HPW), tungstosilicic acid ($H_4SiW_{12}O_{40}$, HSiW), and phosphomolybdic acid ($H_3PMo_{12}O_{40}$, HPMo), are widely employed in various applications [32,39]. In this work, the polyoxometalate cesium salts, which offer advantages over the parent polyoxometalate acids, including larger surface area, higher thermal stability, and insolubility, were employed to anchor Pt precursor ($Pt(acac)_2$) through a deposition-precipitation method [40]. The resultant $Pt_{0.4}/CsPW$, $Pt_{0.4}/CsSiW$, and $Pt_{0.4}/CsPMo$ are white solids, which underwent a H_2-treatment at 250 °C to form the reduced catalysts $Pt_{0.4}/CsPW\text{-}H_2$, $Pt_{0.4}/CsSiW\text{-}H_2$, and $Pt_{0.4}/CsPMo\text{-}H_2$ as gray solids, respectively (Scheme 1). Based on ICP-OES analyses, the Pt weight loading of these catalysts was measured to be approximately 0.4 wt%; however, the molar ratios of Cs to Keggin units varied with the polyoxometalates, ranging from 1.2 to 2.4 (Table S1). The analyses of $Pt_{0.4}/CsPW$ and $Pt_{0.4}/CsPW\text{-}H_2$ by FTIR (Figs. S2), Raman (Fig. S3a), ^{31}P MAS NMR (Fig. S3b), and XRD patterns (Figs. S4) confirmed that they displayed a well-shaped Keggin structure of $[PW_{12}O_{40}]^{3-}$ anion, albeit upon the precipitation and H_2-thermal treatments. Similarly, Keggin structures were also observed in $Pt_{0.4}/CsSiW\text{-}H_2$ and $Pt_{0.4}/CsPMo\text{-}H_2$ catalysts (Figs. S13 and S14). SEM images of all three H_2-reduced catalysts displayed numerous spherical-like particles with an average diameter of 75–90 nm (Figs. 1a-1c, and S5). In HRTEM images (Figs. 1d-1f), well-shaped nanocrystalline particles with a spacing of *ca.* 1.1 nm were observed, which agreed with the cubic Pn3m crystalline structures of polyoxometalates found in XRD patterns (Fig. 1g) [41].

The textural properties were determined by adsorption-desorption isotherms of N_2. $Pt_{0.4}/CsPW\text{-}H_2$, where the molar ratio of Cs/Keggin

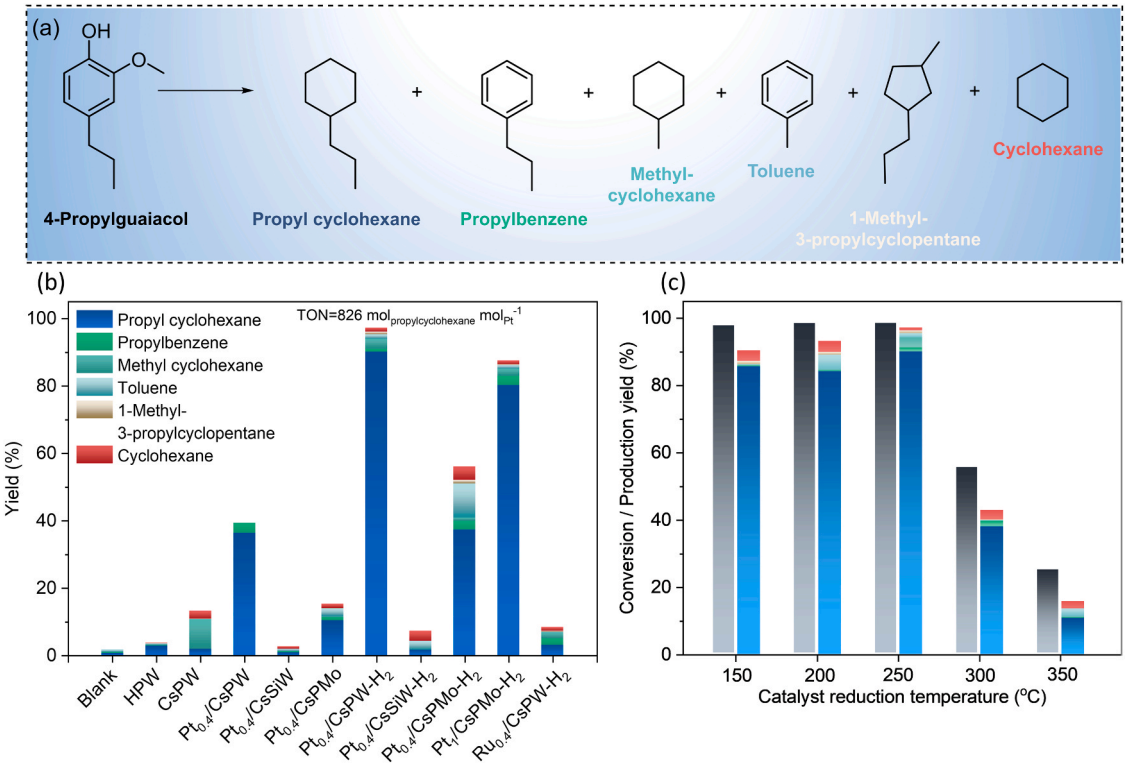

Fig. 4. (a) Products distribution in HDO of 4-propylguaiacol. (b) Catalyst scanning. (c) H_2-reduction temperature of $Pt_{0.4}/CsPW\text{-}H_2$. Reaction conditions: 4-propylguaiacol (1 mmol), n-dodecane (3 mL), catalyst (50 mg), 2.0 MPa H_2, 150 °C and 4 h.

unit was determined as 2.4, exhibited a type IV isotherm for mesoporous structure [42] and a moderate BET-determined surface area of 134.8 m^2/g (Fig. 1h, Table S1 and S2). In contrast, in the case of catalysts having smaller molar ratios of Cs/Keggin unit, such as $Pt_{0.4}/CsPMo\text{-}H_2$ (2.0) and $Pt_{0.4}/CsSiW\text{-}H_2$ (1.2) (Table S1), the type II and III isotherms with lower surface areas of 58.3 m^2/g and 18.4 m^2/g were observed, corresponding to microporous and nonporous structures, respectively [43]. The scenario that the textural properties of polyoxometalate-based catalysts depend on the Cs component content was in line with previous studies [39,44]. The thermogravimetric analyses indicated that no obvious decomposition occurred on CsPW salt and $Pt_{0.4}/CsPW\text{-}H_2$ up to 800 °C, in contrast to $H_3PW_{12}O_{40}$, where the weight loss resulting from the Keggin structure decomposition was observed at 400–500 °C (Fig. S6) [45]. These results demonstrated the excellent stability of the polyoxometalate Cs salt-supported Pt catalysts.

To understand the acidic species and redox properties responsible for HDO reactions, the NH_3-TPD (Fig. 1i), Py-FTIR (Fig. S7), and H_2-TPD experiments (Fig. 1j) were performed. Based on NH_3-TPD measurements, the acidity followed the order $Pt_{0.4}/CsPW\text{-}H_2 \approx Pt_{0.4}/CsPMo\text{-}H_2 > Pt_{0.4}/CsSiW\text{-}H_2$, where $Pt_{0.4}/CsSiW\text{-}H_2$ did not show any strong acid sites (Table S3 and S4) [46]. In the representative H_2-TPD profiles of three reduced catalysts, the low-temperature desorption peaks assigned to reversibly chemisorbed H_2 were observed at relatively low temperatures (*ca.* 100 °C), indicating the existence of weaker hydrogen surface bonds in the catalysts (Fig. 1j) [47,48]. The total H_2 desorption of $Pt_{0.4}/CsPW\text{-}H_2$ was measured as 0.94 mmol/g, being higher than those of $Pt_{0.4}/CsSiW\text{-}H_2$ (0.53 mmol/g) and $Pt_{0.4}/CsPMo\text{-}H_2$ (0.26 mmol/g). Of note, these measured H_2 desorption values have exceeded the theoretical H_2 chemisorption capacities of Pt sites in the catalysts (0.12 mmol/g), because polyoxometalate with the redox potential can serve as an efficient H_2 storage buffer and carrier. This would be highly conducive to HDO reactions [34].

3.2. *Identification of Pt species in $Pt_1/CsPMo\text{-}H_2$*

Attempts to characterize Pt elements in the low-loaded Pt (0.4 wt%) catalysts by HRTEM (Fig. 1a-f), XRD (Fig. 1g), XPS (Fig. S8), and EDX techniques (Fig. S9) were not successful, because Pt species are interfered with the P, W, and Cs elements. Thereby, we fabricated a catalyst with 1 wt%-loaded Pt element ($Pt_1/CsPMo\text{-}H_2$) *via* the same synthetic method.

Pt species in $Pt_1/CsPMo\text{-}H_2$ were spectroscopically measured at the L_3-edge using XANES and EXAFS to unravel its electronic arrangement and coordination configuration. As shown in the XANES spectra, Pt species displayed a significantly lower white line peak intensity than PtO_2 but higher than Pt foil in metallic form (Fig. 2a), suggesting a positive valence state [49]. A comparison was made between the Fourier transforms (FT) of the Pt L_3-edge EXAFS spectra for $Pt_1/CsPMo\text{-}H_2$, Pt foil, and PtO_2 curves, as shown in Fig. 2b. A k_2-weighted FT was utilized to facilitate a visual comparison among different samples. The existence of a notable summit at 1.62 Å in $Pt_1/CsPMo\text{-}H_2$ corresponded to the Pt−O scattering route, with no observation of the peak at 2.52 Å from Pt−Pt contribution. This categorical confirmation established that Pt species in $Pt_1/CsPMo\text{-}H_2$ were in their isolated state [50]. Based on EXAFS wavelet transform (WT) analysis, the coordination conditions of Pt centers in $Pt_1/CsPMo\text{-}H_2$ were further investigated, which provided both radial distance resolution and *k*-space resolution (Fig. 2c and Fig. S12). The Pt L_3-edge WT plots of $Pt_1/CsPMo\text{-}H_2$ exhibited a solitary peak at approximately 1.6 Å, with no discernible intensity corresponding to Pt−Pt interaction observed, confirming again that $Pt_1/CsPMo\text{-}H_2$ exclusively features Pt−O coordination. The first shell curve fitting data indicated that the coordination number (CN) of Pt−O was close to 2 (Table S5), thus suggesting that Pt atom is plausibly anchored as an O_t−Pt−O_{br} coordination bridge site at the 3-fold hollow site of $[PMo_{12}O_{40}]^{3+}$ (Fig. 2f) [29].

EDX mappings of $Pt_1/CsPMo\text{-}H_2$ revealed that Pt elements were highly dispersed, which, together with the absence of Bragg diffraction

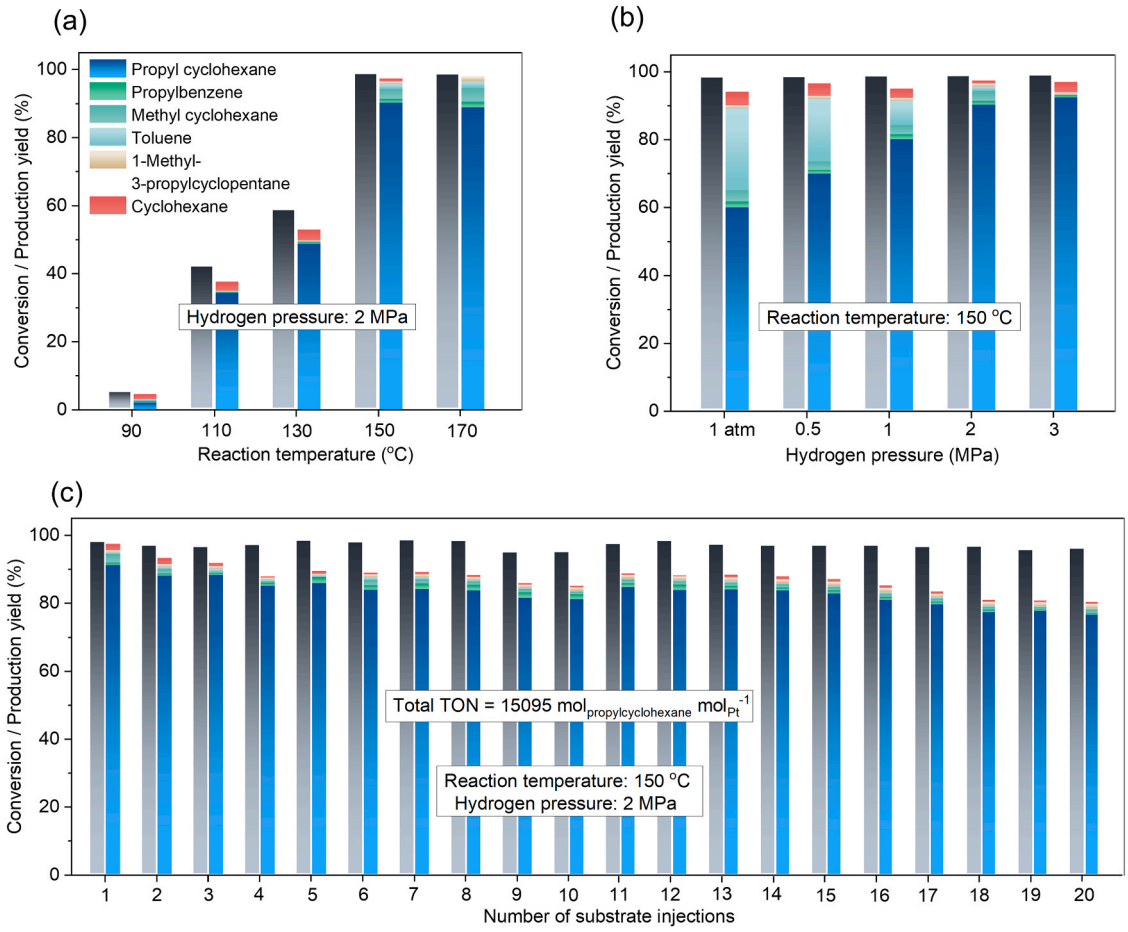

Fig. 5. Optimization of reaction parameters in 4-propylguaiacol HDO reaction including (a) Reaction temperature. (b) Hydrogen pressure. Reaction conditions: 4-propylguaiacol (1 mmol), n-dodecane (3 mL), $Pt_{0.4}/CsPW\text{-}H_2$ (50 mg), 4 h. (c) The performance of the $Pt_{0.4}/CsPW\text{-}H_2$ catalyst with increased injection numbers. Reaction conditions: 4-propylguaiacol (2 mmol), n-dodecane (6 mL), $Pt_{0.4}/CsPW\text{-}H_2$ (100 mg), 2.0 MPa H_2, 150 °C and 4 h.

of Pt from XRD patterns, indicated that Pt species are present in a very small size (Fig. 2g). In HAADF-STEM images, it was difficult to distinguish corresponding metals because Pt, Mo, and Cs elements were all emerged as dense bright spots (Fig. 2d). In a larger version of HAADF-STEM image, the suspected kegging structures could be outlined (Fig. 2e), which was agreed with the calculated Pt coordination number. Given the atomic dispersion state of Pt in the $Pt_1/CsPMo\text{-}H_2$ catalyst, we speculated that Pt species should also exist as single atomic versions in $Pt_{0.4}/CsPW\text{-}H_2$, $Pt_{0.4}/CsSiW\text{-}H_2$, and $Pt_{0.4}/CsPMo\text{-}H_2$ catalysts with lower Pt loading.

3.3. DFT calculation

To anticipate the catalytic activity and validate the structural model of these catalysts, DFT calculations were employed to determine the band gap between the highest occupied molecular orbital (HOMO) and the lowest unoccupied molecular orbital (LUMO) [51]. The atomic structural models of $Pt_{0.4}/CsPW\text{-}H_2$, $Pt_{0.4}/CsSiW\text{-}H_2$, and $Pt_{0.4}/CsPMo\text{-}H_2$ catalysts were schematically illustrated in Fig. 3a. The average bond distance of Pt−O was calculated as 1.95 Å, closely matching the result obtained from EXAFS fitting (2.02 Å) (Table S5). Given the HOMO-LOMO orbital energy gap can demonstrate a robust quantitative correlation with catalytic activity, the molecular orbital energy diagrams of $Pt_{0.4}/CsPW\text{-}H_2$, $Pt_{0.4}/CsSiW\text{-}H_2$, and $Pt_{0.4}/CsPMo\text{-}H_2$ were projected onto the van der Waals surface for HOMO and LUMO using the DMol^3 program (Fig. 3b). In the case of $Pt_{0.4}/CsPW\text{-}H_2$, the calculated HOMO–LUMO band gap (Δ ($E_{LUMO} - E_{HOMO}$)) was 1.201 eV, which was smaller than those of $Pt_{0.4}/CsSiW\text{-}H_2$ (1.257 eV) and $Pt_{0.4}/CsPMo\text{-}H_2$ (1.240 eV). The relatively small band gap of $Pt_{0.4}/CsPW\text{-}H_2$ indicated that it can be more easily activated, thus displaying a higher level of catalytic activity [52,53].

3.4. HDO of 4-propylguaiacol

The catalytic performance of polyoxometalate-supported Pt catalysts was initially assessed by the HDO of a lignin-depolymerized product 4-propylguaiacol (**4-PG**) under conditions of 150 °C and 2 MPa H_2 for 4 h (Fig. 4). The efficiency and selectivity of **4-PG** transformation were dependent on both the active metal centers and the support of the catalysts. Among the screened catalysts, $Pt_{0.4}/CsPW\text{-}H_2$ demonstrated the best catalytic performance, achieving a complete conversion of **4-PG**. In the resultant products, propylcyclohexane formed via dehydroxylation, demethoxylation, and arene hydrogenation [54], was identified as the major product in 91% yield. The TON was calculated as 826 $mol_{propylcyclohexane}$ mol_{Pt}^{-1} under such a transformation (Fig. 4b). Control reactions catalyzed by HPW and CsPW resulted in poor conversions of **4-PG**, illustrating the pivotal role of Pt active centers, albeit with extremely-low loading. As for $Pt_{0.4}/CsPMo\text{-}H_2$ catalyst, a moderate yield of HDO products was generated (56.0%), with 66.6% selectivity to propylcyclohexane. In the case of $Pt_{0.4}/CsSiW\text{-}H_2$, a poor conversion of **4-PG** was observed (9.4%). The above results indicated that the polyoxometalate supports have a great effect on the HDO of **4-PG**. The order of the catalytic performance, that is $Pt_{0.4}/CsPW\text{-}H_2 > Pt_{0.4}/CsPMo\text{-}H_2 > Pt_{0.4}CsSiW\text{-}H_2$, was respectively consistent with the orders of their total acidities, textural properties and H_2 chemisorption capacities. Notably, the sequence of catalytic performance stayed aligned with DFT

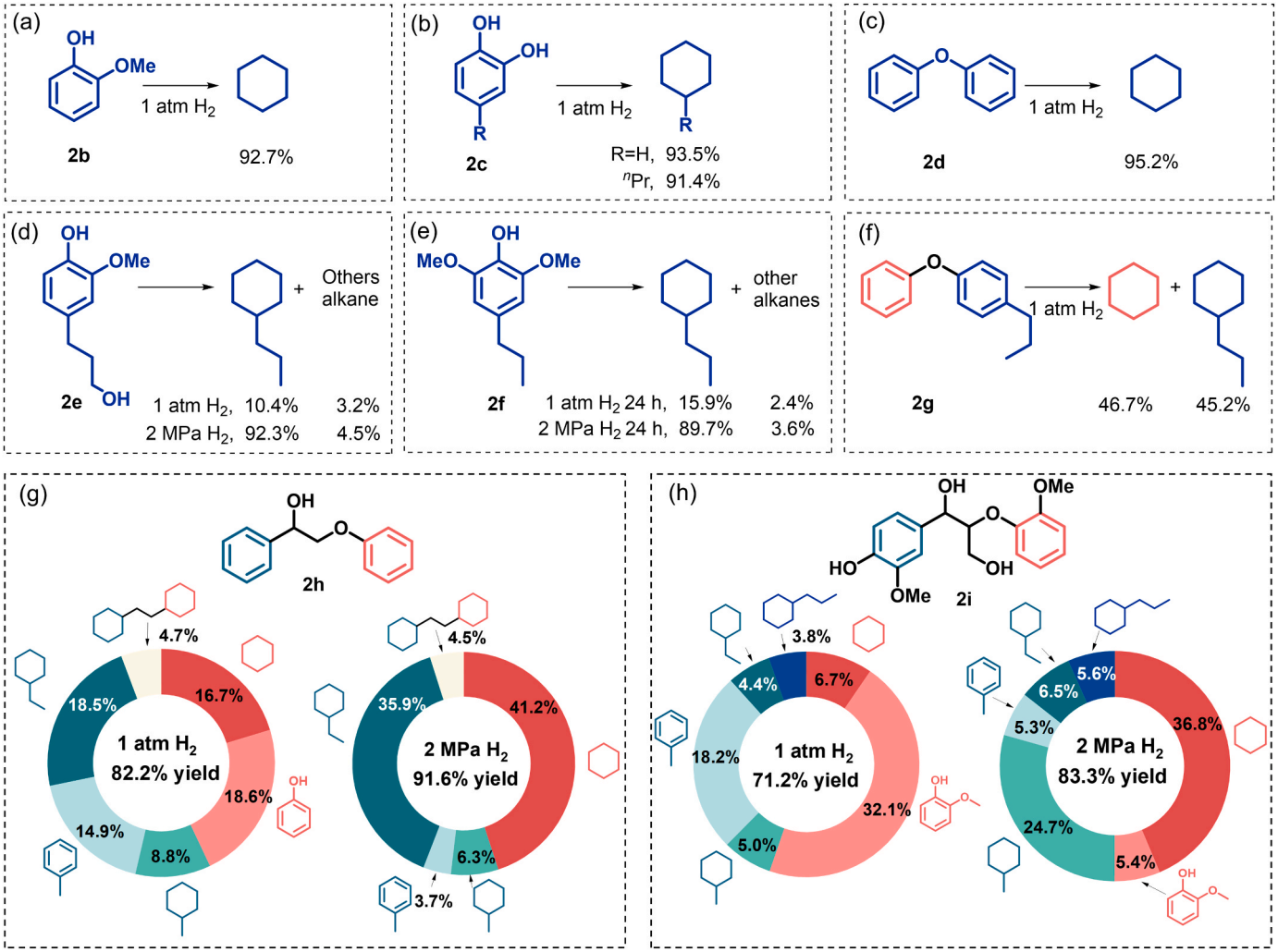

Fig. 6. HDO of phenolic substrates over $Pt_{0.4}$/CsPW-H_2 catalyst. Unless noted otherwise, these reactions were performed at the conditions of substrate (1 mmol), $Pt_{0.4}$/CsPW-H_2 (50 mg), n-dodecane (3 mL), 150 °C, and 10 h.

calculated HOMO–LUMO band gaps (Fig. 3), demonstrating the reliability of predicated catalyst's structures.

In the case of pre-reduced catalysts, decreased HDO efficiencies were observed compared to those of the reduced catalysts, while the catalytic performance followed a similar trend of support effect ($Pt_{0.4}$/CsPW > $Pt_{0.4}$/CsPMo > $Pt_{0.4}$CsSiW). By changing the active metal site from Pt to Ru, $Ru_{0.4}$/CsPW-H_2 delivered a low yield of HDO products (8.4%). Compared to $Pt_{0.4}$/CsPMo-H_2, the higher Pt-loaded catalyst Pt_1/CsPMo-H_2 led to an increase in the yield of HDO products (87.6% vs 56.0%) and the selectivity towards propylcyclohexane (91.6% vs 36.9%). We also screened the reduction temperatures during the preparation of $Pt_{0.4}$/CsPW-H_2 (Fig. 4c). When the reduction temperature was raised to 300 °C and 350 °C, significant declines in **4-PG** conversion were observed (56.2% and 25.7%, respectively), which can be explained by possibly the diffusion of Cs^+ and H^+ at high temperature, thus resulting in the decrease of catalyst activity [41].

The influence of reaction temperature on the HDO of **4-PG** over $Pt_{0.4}$/CsPW-H_2 catalyst was investigated (Fig. 5a). When the reactions were conducted below 150 °C, a drop in HDO product yields was observed, as seen in the case of 130 °C (53%) and 110 °C (37.6%), while the selectivity to propylcyclohexane remained high (92.1% and 91.3%, respectively). Investigations into H_2 pressure effect were performed at 150 °C for 4 h (Fig. 5b). Almost all **4-PG** could be consumed through HDO reaction under varied H_2 pressures, and the product distributions depended on the H_2 pressure. Under 1 atm H_2 pressure, the total yields of hydrocarbons could reach 94.1%, where toluene and propylcyclohexane were parallelly formed in 24.1% and 59.9% yields, respectively. A chemoselectivity switch from toluene to propylcyclohexane was observed with increasing H_2 pressure, and propylcyclohexane was finally formed in 92.3% yield under 3 MPa H_2 pressure. Given that the formation of toluene undergoing hydrodealkylation favored the absence of Pt species (CsPW-catalyzed HDO reaction, Fig. 4b) and low H_2 pressure (Fig. 5b), introducing Pt species and/or increasing H_2 pressure can suppress C–C bond cracking, thereby preserving higher selectivity for C9 products. Compared with previous HDO results that required high reaction temperature and high H_2 pressure [15] [19,20], this study achieved high yields of hydrocarbons at a relatively mild temperature (150 °C) and a low H_2 pressure (1 atm), along with a high ratio of substrate to Pt (909 mol/mol). The high catalytic efficiency of $Pt_{0.4}$/CsPW-H_2 may be associated with the strong acid strength and the redox potential of polyoxometalate support.

Considering the unique "pseudo-liquid phase" of polyoxometalate, continuous injection experiments were performed to test the recyclability and stability of the $Pt_{0.4}$/CsPW-H_2 catalyst. As displayed in Fig. 5c, the conversion of **4-PG** remained over 95% at each interval, with high selectivity to propylcyclohexane in the cumulative products (> 94%). Over 20 additions of **4-PG**, $Pt_{0.4}$/CsPW-H_2 demonstrated good catalytic performance and stability in the 80-h reaction, during which the mol ratio of **4-PG** to Pt reached 18,182 and total TON was calculated as 15095 $mol_{propylcyclohexane}$ mol_{Pt}^{-1}. FTIR spectra were provided for the

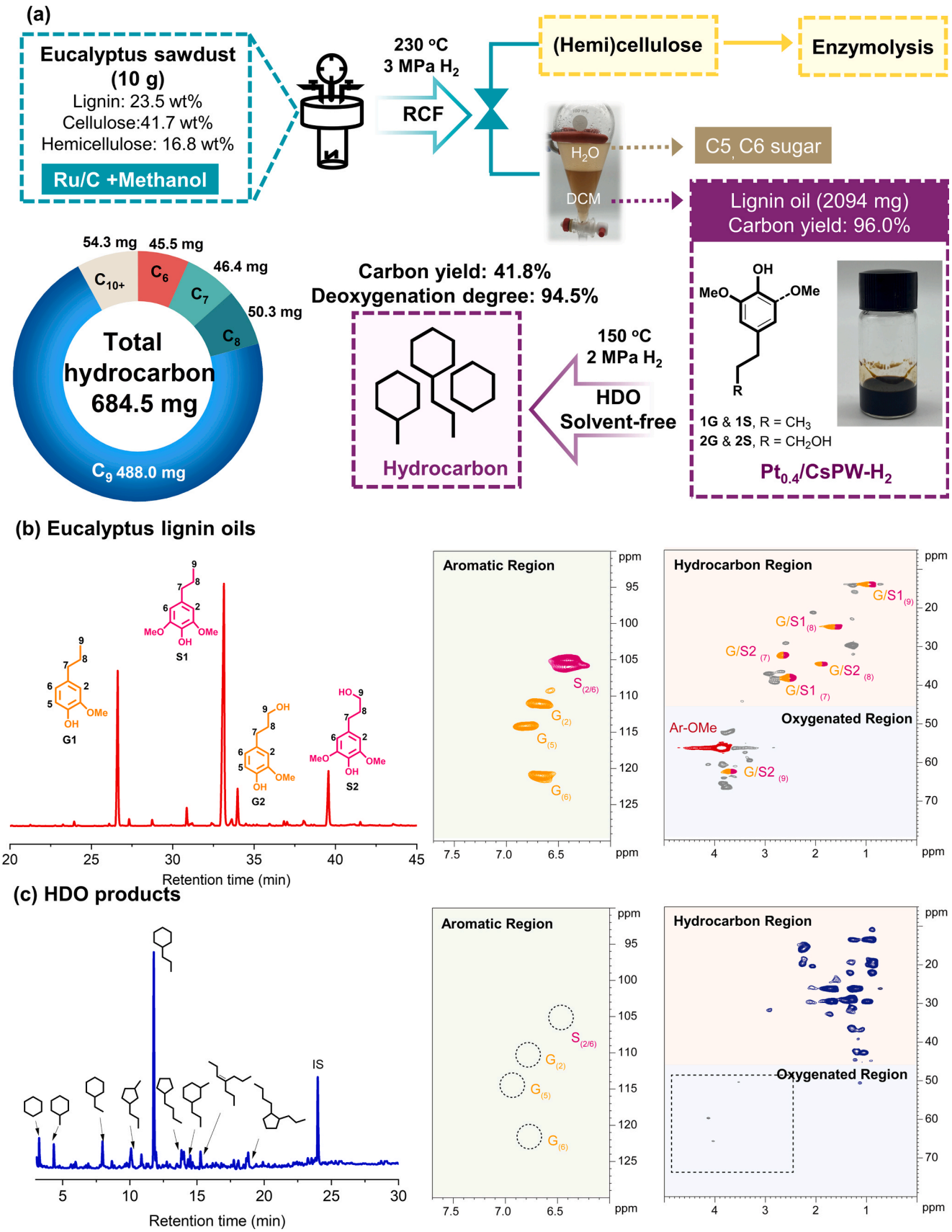

Fig. 7. Lignin-derived biophenolics HDO reaction. (a) Schematic for HDO upgrade process of Eucalyptus wood lignocellulose into hydrocarbons. Gas chromatogram and 2D HSQC NMR spectra of (b) Eucalyptus lignin oils and (c) HDO products.

spent catalyst, showing no obvious changes in Keggin structure of $[PW_{12}O_{40}]^{3-}$ anion (Fig. S2). In the thermogravimetric curves of the spent $Pt_{0.4}$/CsPW-H_2, a second weight loss at 150–350 °C was witnessed, which could be attributed to the pyrolysis of adsorbed organic components on the catalyst (Fig. S6). It was supposed that the slight deactivation should be mainly because of carbonaceous deposition during the catalytic procedure.

3.5. HDO of various lignin-derived phenolic

It has been widely acknowledged that the depolymerization of lignin can lead to the formation of diverse phenolic monomers and dimers [10, 13]. Thereby, some representative lignin-derived compounds with disparate OH, OCH_3, and sidechains were tested over the $Pt_{0.4}$/CsPW-H_2 catalyst (Fig. 6). At 150 °C, guaiacol **2b** can be transformed into cyclohexane in 92.7% yield under 1 atm H_2, showing higher HDO efficiency than **4-PG** with a propyl sidechain. Under such a mild condition, the HDO of catechyl derivatives **2c** (the depolymerized products from C-lignin [55]) afforded cyclohexane and propylcyclohexane in 93.5% and 91.4% yields, respectively. In the case of diphenyl ethers (**2d** and **2 g**) with lignin-contained 4-O-5 structure, the $Pt_{0.4}$/CsPW-H_2 catalyst demonstrated high catalytic performance, resulting in combined yields of 95.2% and 91.9% for cyclohexane derivatives, respectively. When 4-propanol-substituted guaiacol **2e** (a major product from Pd/C-catalyzed hydrogenolysis of lignin [56]) was tested, 1-atm H_2 condition was insufficient to accompany the HDO reaction (13.6% yield). We then increased the H_2 pressure to 2 MPa, under which a high yield of propylcyclohexane (92.3%) was obtained. In the case of 4-propyl syringol **2 f**, the complete HDO could be realized only when H_2 pressure was promoted (2 MPa) and the reaction time was prolonged (24 h), probably because of the steric effects [57].

β-O-4 species, comprising a secondary benzylic alcohol and a primary aliphatic alcohol, are the most abundant structure in lignin biopolymer [58]. Investigations of HDO of β-O-4 dimers by $Pt_{0.4}$/CsPW-H_2 were performed at 150 °C. In the case of **2i**, which has a free phenol group in addition to two methoxy and two alkyl hydroxyl groups, a complete cleavage of β-O-4 linkage was achieved under ambient H_2 pressure, resulting in the formation of cycloalkanes (20.9%), toluene (18.2%) and guaiacol (32.1%) in a combined yield of 71.2%. Increasing the H_2 pressure to 2 MPa significantly enhanced the HDO efficiency, where hydrocarbons became the major products (78%), along with a 5.4% yield of guaiacol. Of note, hydrodealkylation (C−C bond cleavage) occurred at β-O-4 linkage probably due to the high acidity of $Pt_{0.4}$/CsPW-H_2. Similar results were also obtained in the case of dimer **2 h**, from which hydrocarbons were produced with a yield of 91.6%. The above results suggested that $Pt_{0.4}$/CsPW-H_2 catalyst is capable of both the cleavage of lignin linkages and the HDO of lignin monomers.

3.6. HDO of lignin-depolymerized biophenolics

Encouraged by the promising results, direct upgrading of lignin-depolymerized biophenolics to hydrocarbon fuels with the $Pt_{0.4}$/CsPW-H_2 catalyst was investigated. As shown in Fig. 7a, the lignin biophenolics (2094 mg) obtained from Ru/C-catalyzed RCF of Eucalyptus sawdust (10 g) was a dark brown and viscous liquid. Gel permeation chromatography (GPC) analysis of lignin-derived biophenolics gave an average molecular weight (M_w) of 366 g mol^{-1}, where signals ascribed monomers, dimers, and oligomers were all detected (Fig. S16) [59]. By comparison with the authentic samples obtained commercially or synthesized independently, 4-propyl- and 4-propanol-substituted guaiacol/syringol were determined as the major phenolic monomers (1062 mg, *ca.* 5.42 mmol) (Fig. 7b). A series of phenolic dimers were also identified by GC-MS.

HDO of the lignin biophenolics (2094 mg) was carried out over $Pt_{0.4}$/CsPW-H_2 at 150 °C under 2 MPa H_2. Owing to its liquidity, no additional solvent was used for this transformation, which would make for energy consumption and product separation. Total conversion of the oxygenated monomers was achieved after 24 h. GC characterization illustrated that the liquid products were composed of C_6-C_{10} hydrocarbons, with no observation of oxygen-containing products (Fig. 7c). The total mass yield of collected alkanes was measured as 32.7 wt% based on lignin derivatives. Propylcyclohexane was identified as the major product (488.0 mg, 23.3 wt%), together with observation of cyclohexane (45.5 mg, 2.2 wt%), methylcyclohexane (46.4 mg, 2.2 wt%), ethylcyclohexane (50.3 mg, 2.4 wt%), and some C_{10+} alkanes (54.3 mg, 2.6 wt%). The total moles of as-obtained alkanes were calculated as 5.73 mmol, slightly higher than that of the phenolic monomers in original lignin oils (5.42 mmol), suggesting that some dimers and/or oligomers have been transformed into alkanes. The elemental analysis illustrated that the actual oxygen content was decreased from 29.1% for original lignin oils to 1.6% in the upgraded products, corresponding to a 95% deoxygenation degree (Table S10). 2D HSQC NMR spectroscopy experiments were performed to provide a comprehensive visualization of HDO products. The cross signals corresponding to phenyl, guaiacol, and syringyl arenes, as well as the methoxy group, that existed in RCF lignin phenolics (Fig. 7b), were no longer present in HDO products (Fig. 7c), demonstrating an efficient demethoxylation and arene hydrogenation processes. A set of correlation signals appeared in the aliphatic region, attributed to ^{13}C–^{1}H NMR interactions of C_6–C_9 cycloalkanes (Fig. 7c). The prevalence of alkane compounds in 2D NMR spectra aligns with the findings observed in the GC spectrum. These results testified that $Pt_{0.4}$/CsPW-H_2 exhibits significant catalytic activity in converting authentic and intricate lignin phenolics into high-energy-density naphthenic hydrocarbons.

4. Conclusion

In conclusion, we have fabricated a family of polyoxometalate cesium salt-supported, extremely low-loaded Pt catalysts, where Pt species were dispersed in single atoms manner based on experimental characterizations and DFT calculation. The activities of Pt-polyoxometalate for 4-propylguaiacol HDO displayed dependence on their textural property, acidity, and hydrogen storage capacity. The consistency between catalytic performance and DFT calculated HOMO–LUMO band gaps of these catalysts implied the reliability of predicated catalyst's structures. The $Pt_{0.4}$/CsPW-H_2 catalyst demonstrated superior activity, selectivity, and stability for the transformation of 4-propylguaiacol to cyclohexane, which could also drive the HDO of a series of lignin-derived phenolics into hydrocarbons in high yields even at 150 °C and 1 atm H_2 conditions. Moreover, this catalyst also showed high activity in the HDO of lignin oils from Eucalyptus wood, thus resulting in cycloalkane products (C_6-C_{10}) in a high yield (33% by weight) with impressive deoxygenation degree (95%). This study represented a significant advancement in the development of efficient catalysts for the transformation of lignin-derived bio-phenolics into hydrocarbons under relatively mild conditions.

CRediT authorship contribution statement

Rumin Ma: Visualization, Software. **Zhenzhen Liu:** Formal analysis, Data curation. **Xueying Gao:** Writing – original draft, Visualization, Data curation. **Guoyong Song:** Writing – review & editing, Funding acquisition, Conceptualization. **Shuizhong Wang:** Validation, Software. **Yulong Wu:** Writing – review & editing, Resources.

Declaration of Competing Interest

There are no conflicts of interest to declare.

Data availability

Data will be made available on request.

Acknowledgments

This work was supported by the National Key Research and Development Program of China (No. 2019YFC1906700), the National Natural Science Foundation of China (No. 31971607).

Appendix A. Supporting information

Supplementary data associated with this article can be found in the online version at doi:10.1016/j.apcatb.2024.124059.

References

[1] A.R.C. Morais, A.M. da Costa Lopes, R. Bogel-Łukasik, Carbon dioxide in biomass processing: contributions to the green biorefinery concept, Chem. Rev. 115 (2015) 3–27, https://doi.org/10.1021/cr500330z.
[2] Y. Zhang, Carbon dioxide utilization: a carbon-neutral energy cycle, Nat. Rev. Chem. 1 (2017) 0057, https://doi.org/10.1038/s41570-017-0057.
[3] M. Fajardy, S. Chiquier, N. Mac Dowell, Investigating the BECCS resource nexus: delivering sustainable negative emissions, Energy Environ. Sci. 11 (2018) 3408–3430, https://doi.org/10.1039/C8EE01676C.
[4] Z. Sun, G. Bottari, A. Afanasenko, M.C.A. Stuart, P.J. Deuss, B. Fridrich, K. Barta, Complete lignocellulose conversion with integrated catalyst recycling yielding valuable aromatics and fuels, Nat. Catal. 1 (2018) 82–92, https://doi.org/10.1038/s41929-017-0007-z.
[5] L. Faba, E. Díaz, S. Ordóñez, Recent developments on the catalytic technologies for the transformation of biomass into biofuels: a patent survey, Renew. Sustain. Energy Rev. 51 (2015) 273–287, https://doi.org/10.1016/j.rser.2015.06.020.
[6] J. Zakzeski, P.C.A. Bruijnincx, A.L. Jongerius, B.M. Weckhuysen, The catalytic valorization of lignin for the production of renewable chemicals, Chem. Rev. 110 (2010) 3552–3599, https://doi.org/10.1021/cr900354u.
[7] M.V. Galkin, J.S.M. Samec, Lignin valorization through catalytic lignocellulose fractionation: a Fundamental platform for the future biorefinery, ChemSusChem 9 (2016) 1544–1558, https://doi.org/10.1002/cssc.201600237.
[8] R.-C. Sun, Lignin source and structural characterization, ChemSusChem 13 (2020) 4385–4393, https://doi.org/10.1002/cssc.202001324.
[9] A.J. Ragauskas, G.T. Beckham, M.J. Biddy, R. Chandra, F. Chen, M.F. Davis, B. H. Davison, R.A. Dixon, P. Gilna, M. Keller, P. Langan, A.K. Naskar, J.N. Saddler, T. J. Tschaplinski, G.A. Tuskan, C.E. Wyman, Lignin valorization: improving lignin processing in the biorefinery, Science 344 (2014) 1246843, https://doi.org/10.1126/science.1246843.
[10] Z. Liu, H. Li, X. Gao, X. Guo, S. Wang, Y. Fang, G. Song, Rational highly dispersed ruthenium for reductive catalytic fractionation of lignocellulose, Nat. Commun. 13 (2022) 4716, https://doi.org/10.1038/s41467-022-32451-5.
[11] Z. Sun, B. Fridrich, A. de Santi, S. Elangovan, K. Barta, Bright side of lignin depolymerization: toward new platform chemicals, Chem. Rev. 118 (2018) 614–678, https://doi.org/10.1021/acs.chemrev.7b00588.
[12] S. Van den Bosch, W. Schutyser, R. Vanholme, T. Driessen, S.F. Koelewijn, T. Renders, B. De Meester, W.J.J. Huijgen, W. Dehaen, C.M. Courtin, B. Lagrain, W. Boerjan, B.F. Sels, Reductive lignocellulose fractionation into soluble lignin-derived phenolic monomers and dimers and processable carbohydrate pulps, Energy Environ. Sci. 8 (2015) 1748–1763, https://doi.org/10.1039/C5EE00204D.
[13] H. Dao Thi, K. Van Aelst, S. Van den Bosch, R. Katahira, G.T. Beckham, B.F. Sels, K. M. Van Geem, Identification and quantification of lignin monomers and oligomers from reductive catalytic fractionation of pine wood with GC × GC – FID/MS, Green Chem. 24 (2022) 191–206, https://doi.org/10.1039/D1GC03822B.
[14] X. Diao, N. Ji, X. Li, Y. Rong, Y. Zhao, X. Lu, C. Song, C. Liu, G. Chen, L. Ma, S. Wang, Q. Liu, C. Li, Fabricating high temperature stable Mo-Co_9S_8/Al_2O_3 catalyst for selective hydrodeoxygenation of lignin to arenes, Appl. Catal. B-Environ. 305 (2022) 121067, https://doi.org/10.1016/j.apcatb.2022.121067.
[15] Z. Cao, M. Dierks, M.T. Clough, I.B. Daltro de Castro, R. Rinaldi, A convergent approach for a deep converting lignin-first biorefinery rendering high-energy-density drop-in fuels, Joule 2 (2018) 1118–1133, https://doi.org/10.1016/j.joule.2018.03.012.
[16] K. Wu, W. Wang, H. Guo, Y. Yang, Y. Huang, W. Li, C. Li, Engineering Co nanoparticles Supported on defect MoS_{2-x} for mild deoxygenation of lignin-derived phenols to arenes, ACS Energy Lett. 5 (2020) 1330–1336, https://doi.org/10.1021/acsenergylett.0c00411.
[17] W. Guan, X. Chen, C.W. Tsang, H. Hu, C. Liang, Highly dispersed Rh/NbOx invoking high catalytic performances for the valorization of lignin monophenols and lignin oil into aromatics, ACS Sustain. Chem. Eng. 9 (2021) 3529–3541, https://doi.org/10.1021/acssuschemeng.0c08478.
[18] L. Dong, Y. Xin, X. Liu, Y. Guo, C.-W. Pao, J.-L. Chen, Y. Wang, Selective hydrodeoxygenation of lignin oil to valuable phenolics over Au/Nb_2O_5 in water, Green Chem. 21 (2019) 3081–3090, https://doi.org/10.1039/C9GC00327D.
[19] G.-H. Wang, Z. Cao, D. Gu, N. Pfänder, A.-C. Swertz, B. Spliethoff, H.-J. Bongard, C. Weidenthaler, W. Schmidt, R. Rinaldi, F. Schüth, Nitrogen-doped ordered mesoporous carbon supported bimetallic ptco nanoparticles for upgrading of biophenolics, Angew. Chem. Int. Ed. 55 (2016) 8850–8855, https://doi.org/10.1002/anie.201511558.
[20] A. Bjelić, M. Grilc, M. Huš, B. Likozar, Hydrogenation and hydrodeoxygenation of aromatic lignin monomers over Cu/C, Ni/C, Pd/C, Pt/C, Rh/C and Ru/C catalysts: Mechanisms, reaction micro-kinetic modelling and quantitative structure-activity relationships, Chem. Eng. J. 359 (2019) 305–320, https://doi.org/10.1016/j.cej.2018.11.107.
[21] X. Zhang, Q. Zhang, T. Wang, L. Ma, Y. Yu, L. Chen, Hydrodeoxygenation of lignin-derived phenolic compounds to hydrocarbons over Ni/SiO_2–ZrO_2 catalysts, Bioresour. Technol. 134 (2013) 73–80, https://doi.org/10.1016/j.biortech.2013.02.039.
[22] K. Wu, X. Li, W. Wang, Y. Huang, Q. Jiang, W. Li, Y. Chen, Y. Yang, C. Li, Creating edge sites within the basal plane of a MoS_2 catalyst for substantially enhanced hydrodeoxygenation activity, ACS Catal. 12 (2022) 8–17, https://doi.org/10.1021/acscatal.1c03669.
[23] X. Gao, H. Li, S. Wang, Z. Liu, J.-f Ma, X.-e Liu, G. Song, Hydrodeoxygenation of lignin biophenolics to cyclohexanes over sub-nanometric Ru multifunctional catalyst, Renew. Energy 201 (2022) 724–733, https://doi.org/10.1016/j.renene.2022.10.090.
[24] H. Wang, J. Male, Y. Wang, Recent advances in hydrotreating of pyrolysis bio-oil and its oxygen-containing model compounds, ACS Catal. 3 (2013) 1047–1070, https://doi.org/10.1021/cs400069z.
[25] D. Lachos-Perez, P. César Torres-Mayanga, E.R. Abaide, G.L. Zabot, F. De Castilhos, Hydrothermal carbonization and liquefaction: differences, progress, challenges, and opportunities, Bioresour. Technol. 343 (2022) 126084, https://doi.org/10.1016/j.biortech.2021.126084.
[26] J. Zhong, J. Pérez-Ramírez, N. Yan, Biomass valorisation over polyoxometalate-based catalysts, Green Chem. 23 (2021) 18–36, https://doi.org/10.1039/D0GC03190A.
[27] K. Alharbi, W. Alharbi, E.F. Kozhevnikova, I.V. Kozhevnikov, Deoxygenation of ethers and esters over bifunctional Pt–heteropoly acid catalyst in the gas phase, ACS Catal. 6 (2016) 2067–2075, https://doi.org/10.1021/acscatal.6b00096.
[28] H. Althikrallah, E.F. Kozhevnikova, I.V. Kozhevnikov, Facile gas-phase hydrodeoxygenation of 2,5-dimethylfuran over bifunctional metal-acid catalyst Pt–$Cs_{2.5}H_{0.5}PW_{12}O_{40}$, Chem. Commun. 57 (2021) 227–230, https://doi.org/10.1039/D0CC06934E.
[29] B. Zhang, G. Sun, S. Ding, H. Asakura, J. Zhang, P. Sautet, N. Yan, Atomically dispersed Pt_1–polyoxometalate catalysts: how does metal–support interaction affect stability and hydrogenation activity? J. Am. Chem. Soc. 141 (2019) 8185–8197, https://doi.org/10.1021/jacs.9b00486.
[30] K. Alharbi, E.F. Kozhevnikova, I.V. Kozhevnikov, Hydrogenation of ketones over bifunctional Pt-heteropoly acid catalyst in the gas phase, Appl. Catal. A-Gen. 504 (2015) 457–462, https://doi.org/10.1016/j.apcata.2014.10.032.
[31] O. Poole, K. Alharbi, D. Belic, E.F. Kozhevnikova, I.V. Kozhevnikov, Hydrodeoxygenation of 3-pentanone over bifunctional Pt-heteropoly acid catalyst in the gas phase: enhancing effect of gold, Appl. Catal. B-Environ. 202 (2017) 446–453, https://doi.org/10.1016/j.apcatb.2016.09.044.
[32] T. Okuhara, N. Mizuno, M. Misono, Catalytic chemistry of heteropoly compounds, in: D.D. Eley, W.O. Haag, B. Gates (Eds.), Adv Catal, Academic Press, 1996, pp. 113–252.
[33] I.V. Kozhevnikov, Catalysis by heteropoly acids and multicomponent polyoxometalates in liquid-phase reactions, Chem. Rev. 98 (1998) 171–198, https://doi.org/10.1021/cr960400y.
[34] W. Liu, W. You, W. Sun, W. Yang, A. Korde, Y. Gong, Y. Deng, Ambient-pressure and low-temperature upgrading of lignin bio-oil to hydrocarbons using a hydrogen buffer catalytic system, Nat. Energy 5 (2020) 759–767, https://doi.org/10.1038/s41560-020-00680-x.
[35] A.L. Jongerius, J.R. Copeland, G.S. Foo, J.P. Hofmann, P.C.A. Bruijnincx, C. Sievers, B.M. Weckhuysen, Stability of Pt/γ-Al_2O_3 catalysts in lignin and lignin model compound solutions under liquid phase reforming reaction conditions, ACS Catal. 3 (2013) 464–473, https://doi.org/10.1021/cs300684y.
[36] B. Delley, An all-electron numerical method for solving the local density functional for polyatomic molecules, J. Chem. Phys. 92 (1990) 508–517, https://doi.org/10.1063/1.458452.
[37] B. Delley, From molecules to solids with the $DMol^3$ approach, J. Chem. Phys. 113 (2000) 7756–7764, https://doi.org/10.1063/1.1316015.
[38] J.P. Perdew, K. Burke, M. Ernzerhof, Generalized gradient approximation made simple, Phys. Rev. Lett. 77 (1996) 3865–3868, https://doi.org/10.1103/PhysRevLett.77.3865.
[39] M. Misono, Unique acid catalysis of heteropoly compounds (heteropolyoxometalates) in the solid state, Chem. Commun. (2001) 1141–1152, https://doi.org/10.1039/B102573M.
[40] A.V. Anyushin, A. Kondinski, T.N. Parac-Vogt, Hybrid polyoxometalates as post-functionalization platforms: from fundamentals to emerging applications, Chem. Soc. Rev. 49 (2020) 382–432, https://doi.org/10.1039/C8CS00854J.
[41] A. Corma, A. Martínez, C. Martínez, Acidic Cs^+, NH^{4+}, and K^+ Salts of 12-tungstophosphoric acid as solid catalysts for isobutane/2-butene alkylation, J. Catal. 164 (1996) 422–432, https://doi.org/10.1006/jcat.1996.0398.
[42] C. Buttersack, Modeling of type IV and V sigmoidal adsorption isotherms, PCCP 21 (2019) 5614–5626, https://doi.org/10.1039/C8CP07751G.
[43] F. Li, L.J. France, Z. Cai, Y. Li, S. Liu, H. Lou, J. Long, X. Li, Catalytic transfer hydrogenation of butyl levulinate to γ-valerolactone over zirconium phosphates with adjustable Lewis and Brønsted acid sites, Appl. Catal. B-Environ. 214 (2017) 67–77, https://doi.org/10.1016/j.apcatb.2017.05.013.

[44] L. Pesaresi, D.R. Brown, A.F. Lee, J.M. Montero, H. Williams, K. Wilson, Cs-doped $H_4SiW_{12}O_{40}$ catalysts for biodiesel applications, Appl. Catal. A-Gen. 360 (2009) 50–58, https://doi.org/10.1016/j.apcata.2009.03.003.
[45] P.J.M. Carrott, R.A. Roberts, K.S.W. Sing, Adsorption of nitrogen by porous and non-porous carbons, Carbon 25 (1987) 59–68, https://doi.org/10.1016/0008-6223(87)90040-6.
[46] R. Weingarten, Y.T. Kim, G.A. Tompsett, A. Fernández, K.S. Han, E.W. Hagaman, W.C. Conner, J.A. Dumesic, G.W. Huber, Conversion of glucose into levulinic acid with solid metal(IV) phosphate catalysts, J. Catal. 304 (2013) 123–134, https://doi.org/10.1016/j.jcat.2013.03.023.
[47] S. Gholami, S.M. Alavi, M. Rezaei, CO_2 methanation over nanocrystalline Ni catalysts supported on mechanochemically synthesized Cr_2O_3-M (M=Fe, Co, La, and Mn) carriers, Int. J. Hydrog. Energy 46 (2021) 35571–35584, https://doi.org/10.1016/j.ijhydene.2021.08.112.
[48] M. Mihet, G. Blanita, M. Dan, L. Barbu-Tudoran, M.D. Lazar, Pt/UiO-66 nanocomposites as catalysts for CO_2 methanation process, J. Nanosci. Nanotechnol. 19 (2019) 3187–3196, https://doi.org/10.1166/jnn.2019.16607.
[49] H. Yan, M. Zhao, X. Feng, S. Zhao, X. Zhou, S. Li, M. Zha, F. Meng, X. Chen, Y. Liu, D. Chen, N. Yan, C. Yang, PO_4^{3-} Coordinated robust single-atom platinum catalyst for selective polyol oxidation**, Angew. Chem. Int. Ed. 61 (2022) e202116059, https://doi.org/10.1002/anie.202116059.
[50] T. Cui, L. Ma, S. Wang, C. Ye, X. Liang, Z. Zhang, G. Meng, L. Zheng, H.-S. Hu, J. Zhang, H. Duan, D. Wang, Y. Li, Atomically dispersed Pt–N_3C_1 sites enabling efficient and selective electrocatalytic C–C bond cleavage in lignin models under ambient conditions, J. Am. Chem. Soc. 143 (2021) 9429–9439, https://doi.org/10.1021/jacs.1c02328.
[51] S.R. Pilli, T. Banerjee, K. Mohanty, HOMO–LUMO energy interactions between endocrine disrupting chemicals and ionic liquids using the density functional theory: evaluation and comparison, J. Mol. Liq. 207 (2015) 112–124, https://doi.org/10.1016/j.molliq.2015.03.019.
[52] J. Yi, W. Yang, W.-H. Sun, Quantitative Investigation of the electronic and steric influences on ethylene oligo/polymerization by 2-azacyclyl-6-aryliminopyridyl-metal (Fe, Co, and Cr) complexes, Macromol. Chem. Phys. 217 (2016) 757–764, https://doi.org/10.1002/macp.201500429.
[53] Z. Morgan Chan, D.A. Kitchaev, J. Nelson Weker, C. Schnedermann, K. Lim, G. Ceder, W. Tumas, M.F. Toney, D.G. Nocera, Electrochemical trapping of metastable Mn^{3+} ions for activation of MnO_2 oxygen evolution catalysts, Proc. Natl. Acad. Sci. USA 115 (2018) E5261–E5268, https://doi.org/10.1073/pnas.1722235115.
[54] K. Lee, G.H. Gu, C.A. Mullen, A.A. Boateng, D.G. Vlachos, Guaiacol Hydrodeoxygenation mechanism on Pt(111): insights from density functional theory and linear free energy relations, ChemSusChem 8 (2015) 315–322, https://doi.org/10.1002/cssc.201402940.
[55] S. Wang, K. Zhang, H. Li, L.-P. Xiao, G. Song, Selective hydrogenolysis of catechyl lignin into propenylcatechol over an atomically dispersed ruthenium catalyst, Nat. Commun. 12 (2021) 416, https://doi.org/10.1038/s41467-020-20684-1.
[56] S. Van den Bosch, W. Schutyser, S.F. Koelewijn, T. Renders, C.M. Courtin, B.F. Sels, Tuning the lignin oil OH-content with Ru and Pd catalysts during lignin hydrogenolysis on birch wood, Chem. Commun. 51 (2015) 13158–13161, https://doi.org/10.1039/C5CC04025F.
[57] G.S. Foo, A.K. Rogers, M.M. Yung, C. Sievers, Steric effect and evolution of surface species in the hydrodeoxygenation of bio-oil model compounds over Pt/HBEA, ACS Catal. 6 (2016) 1292–1307, https://doi.org/10.1021/acscatal.5b02684.
[58] B.M. Upton, A.M. Kasko, Strategies for the conversion of lignin to high-value polymeric materials: review and perspective, Chem. Rev. 116 (2016) 2275–2306, https://doi.org/10.1021/acs.chemrev.5b00345.
[59] S. Van den Bosch, T. Renders, S. Kennis, S.F. Koelewijn, G. Van den Bossche, T. Vangeel, A. Deneyer, D. Depuydt, C.M. Courtin, J.M. Thevelein, W. Schutyser, B. F. Sels, Integrating lignin valorization and bio-ethanol production: on the role of Ni-Al_2O_3 catalyst pellets during lignin-first fractionation, Green Chem. 19 (2017) 3313–3326, https://doi.org/10.1039/C7GC01324H.